Heliyon 11 (2025) e41875

Contents lists available at ScienceDirect

Heliyon

journal homepage: www.cell.com/heliyon

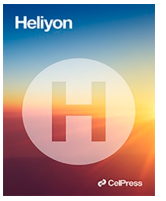

Research article

Chitosan nanoparticles loaded with *Lactobacillus rhamnosus* bioactive metabolites: Preparation, characterization, and antifungal activity

Aya Abdel-Nasser [a,*], Hayam M. Fathy [b], Ahmed N. Badr [a], Olfat S. Barakat [b], Amal S. Hathout [a]

[a] *Food Toxicology and Contaminants Department, National Research Centre, Egypt*
[b] *Agricultural Microbiology Department, Faculty of Agriculture, Cairo University, Egypt*

ARTICLE INFO

Keywords:
Aspergillus flavus
Bioactive metabolites
Chitosan
Lactobacillus rhamnosus
Maize kernels

ABSTRACT

Aspergillus flavus is a severe danger to worldwide maize (*Zea mays*) cultivation, due to its extreme toxicity of aflatoxins produced by the fungi, and its ability to cause economic losses while also posing a health concern to humans and animals. Among the measures that may be considered for *A. flavus* control, applying coatings based on natural ingredients appears to be the most promising. The current work examines the antagonistic ability of *Lactobacillus rhamnosus* bioactive metabolites added to chitosan nanoparticles against *A. flavus* on maize kernels. The chitosan nanoparticles loaded with *L. rhamnosus* bioactive metabolites were characterized using the transmission electron microscope (TEM), zeta potential, size distribution, polydiversity index (PDI), pH, encapsulation efficiency and Fourier transform infrared spectroscopy (FTIR). The TEM revealed that the chitosan nanoparticles loaded with bioactive metabolites were spherical and smooth on the surface, and by increasing the concentration of bioactive metabolites added to the chitosan nanoparticles, the diameter of the chitosan nanoparticle grew. The zeta potential and size distribution values increased as the quantity of *L. rhamnosus* bioactive metabolites increased in the chitosan nanoparticles. The FTIR analysis indicated the presence of several functional groups, including alkynes, alkene, aliphatic primary amines, and other functional groups. The chitosan nanoparticles loaded with *L. rhamnosus* bioactive metabolites at a concentration of 7 mg/mL showed significant antifungal activity against *A. flavus*, reducing their growth in maize kernels by 89.42 % after 10 days of storage. They also reduced the percentage of germination inhibition rate and viability percentage. It could be concluded that adding *L. rhamnosus* bioactive metabolites to chitosan nanoparticles might have significant implications for food safety by using it in the industry to reduce the fungal contamination of grains.

1. Introduction

Corn, sometimes referred to as maize (*Zea mays* L.), is a widely accepted staple in both human and animal diets [1]. It is the cereal plant with the most significant global output and ranks third among staple foods, behind wheat and rice [2]. Previous research showed

* Corresponding author. Food Toxicology and Contaminants Department, National Research Centre, Dokki, Cairo, Egypt.
E-mail addresses: ay.abdelnassser@nrc.sci.eg, ayaabdelnasser85@gmail.com (A. Abdel-Nasser).

https://doi.org/10.1016/j.heliyon.2025.e41875
Received 1 December 2023; Received in revised form 29 December 2024; Accepted 9 January 2025
Available online 10 January 2025

that mycotoxins might easily contaminate maize during all phases of the process, from the field to the table, including the preharvest, harvesting, drying, and postharvest phases, thus posing a major risk to human health and resulting in substantial economic losses [3,4]. Maize is one of the most vulnerable crops to *Aspergillus flavus* infection, which may lead to aflatoxin contamination and threaten the safety of the harvested crops, making it a substantial source of human exposure to mycotoxin [5]. *Aspergillus flavus* is known to modify the biochemical components and mycotoxin contamination in maize kernels during processing and storage, decreasing the likelihood that maize will be used in food products and jeopardizing food safety [1]. Overall, maize contamination by *A. flavus* can occur both before and during harvest [6], whereas certain *Aspergillus* species, known as "storage fungi," are extremely active during storage due to harsh conditions (temperature and water activity),

Aflatoxins (AFs) produced by *Aspergillus flavus* and *Aspergillus parasiticus*, are known to be mutagenic, carcinogenic, and teratogenic [7]. Among the AFs, aflatoxin B_1 (AFB_1), was classified as a Group I human carcinogen by the International Agency for Research on Cancer, and thus has received global attention [8]. Aflatoxins can have serious toxicological consequences on humans and animals and generate significant economic losses for farmers [9]. Treatment of *A. flavus* contamination can significantly decrease or even eliminate significant toxicological implications to both humans and animals, as well as economic losses [10], thus novel eco-friendly and sustainable ways are needed to manage and prevent fungal growth and mycotoxin production.

Nanotechnology is used for the management of nanoparticles for numerous purposes, which serve a critical role in the food and agricultural sectors, boost food quality and safety, and enhance human health through creative and inventive techniques [11]. Biopolymer nanoparticles are widely regarded for their biodegradability, biocompatibility, and non-toxicity [12]. Chitosan ((1 → 4)-2-amino-2-deoxy-β-d-glucose)) is an abundant marine-based biopolymer, and its nanoparticles have been shown to have wide antimicrobial activities against phytopathogenic fungi [13] and stimulate defense in crops [14]. Chitosan nanoparticles are often generated via ionotropic gelation with sodium tripolyphosphate, which is regarded as safe, resulting in nanoparticles with varying sizes, stability, and biological properties, which affect its extensive applicability in agriculture [15]. Chitosan is generally regarded as a low-toxicity material, though its toxicity may vary depending on its physicochemical properties and the experimental model used [16]. It is a biodegradable, and biocompatible polysaccharide that can create films that bind various substances [17]. In recent years, edible coatings involving natural and active chemicals to food surfaces in the form of thin films, have potentially increased the shelf life and improved the quality of food products with long shelf lives that meet consumer expectations [18]. One of the primary benefits of these chitosan films is that they allow for the delayed and regulated migration of bioactive compounds from the chitosan coating into the products [19]. Only a few research have examined the influence of chitosan on fungal growth and mycotoxin production in various fungus species [20,21].

Microbial bioactive metabolites (antibiotics, siderophores, immune-suppressants, enzymes, vitamins and alkaloids) are the naturally active components produced by many bacteria, whereas these bioactive metabolites are produced in trace amounts by microbiota but have high-grade applications such as antibacterial, antitumor, antifungal, and so on [22]; thus, these bioactive compounds are well known to be useful in disciplines such as medicine science, biochemistry, and the food and agriculture industries [23]. Research has been done using biocontrol agents to prevent the development of fungal spoilage and their mycotoxins in food. This procedure, known as "bio-preservation," primarily entails using microorganisms or their metabolites (such as lactic acid and bacteriocin) to extend the shelf life and increase the safety of food products [24].

In our recent study, we extracted and identified bioactive metabolites from *Lactobacillus rhamnosus*, and found that these bioactive metabolites produced various organic acids, volatile organic compounds, and polyphenols and displayed antifungal activity against *A. flavus* and reduced AFB_1 production by 99.98 % [25]. Therefore, this study aimed to evaluate the possibility of controlling *A. flavus* growth in maize kernels by chitosan nanoparticles loaded with *L. rhamnosus* bioactive metabolites.

2. Materials and methods

2.1. Chemicals

Chitosan powder and ethyl acetate HPLC grade were obtained from Merck KGaA (Darmstadt, Germany), whereas lactic acid was obtained from SDFCL Sd Fine Chem Limited (Mumbai, 400 013, India). Sodium sulfate anhydrous, sucrose, and yeast extract were purchased from Loba Chemie (Mumbai 400 005, India). Potato Dextrose agar (PDA) was purchased from Neogen (Lansing, MI 48 912, USA).

2.2. Microorganisms

The *Aspergillus flavus* used in this study was isolated from maize samples in Egypt [26], and the gene sequence was deposited in the GenBank database as *A. flavus* AAM2020 (Accession No. OP942201). *Lactobacillus rhamnosus* ATCC 7469 was obtained from the Microbiological Resources Centre (MIRCEN), Faculty of Agriculture, Ain Shams University.

2.3. Extraction of bacterial bioactive metabolites

Lactobacillus rhamnosus was grown on rice medium (100 g rice in 100 mL distilled water) and incubated in a static condition at 35 °C for 7 days. Ethyl acetate was added at a ratio of 1:1 (v/v) to the rice medium. The ethyl acetate mixtures were poured into separating funnels and allowed to stand until organic and aqueous phases were separated. The organic phase was collected and passed over anhydrous sodium sulfate. This process was repeated three times, and the ethyl acetate was evaporated employing a rotary evaporator

(Heidolph Instruments GmbH & Co. KG, Germany) to yield the extract [25,27].

2.4. Preparation of chitosan nanoparticles

With a few minor adjustments, the primary coating film was created using the techniques previously described by Yadav and Yadav [28]. Briefly, chitosan powder was dissolved in a 1 % aqueous lactic acid solution and well-stirred at 200 rpm for an entire night at room temperature. Glycerol (1 %) was added after complete dissolution, and it was agitated constantly for 4 h. Then, while stirring, a sodium tri-poly phosphate solution (1 mg/mL) was gradually added to the emulsion for an additional hour.

Different L. *rhamnosus* bioactive metabolites 5, 7, and 9 mg/mL concentrations were gradually added to the chitosan nanoparticles and homogenized for 10 min (IKA T-25 Ultra-Turrax Digital High-Speed Homogenizer Systems, IKA®-Werke GmbH and Co. KG, Staufen 79219, Germany). Then, the chitosan nanoparticles loaded with bioactive metabolites were exposed to ultra-sonication (ultra-sonication at 160 W powers, 20 kHz frequency, 50 % pulse, Sonic Ruptor 400, OMNI International) (Fig. 1).

2.5. Characterization of chitosan nanoparticles

2.5.1. Transmission electron microscope (TEM)

The JEOL JEM-2100 a versatile and high-performance High-Resolution Transmission Electron Microscope (HR-TEM, Tokyo 100-0004, Japan) with an acceleration voltage of 120 kV, 600,000× magnification power, a CCD camera was used to characterize the morphology of the particle shape and particle size of the chitosan nanoparticles. A drop of nanoparticle suspension was placed on a carbon-coated copper grid. The grid was dried under an ambient temperature vacuum and investigated under TEM [19].

2.5.2. Zeta potential, size distribution, and polydispersibility index (PDI)

The zeta potential was determined by phase analysis light scattering (PALS) with a Zetasizer NanoZS laser diffractometer (Malvern Panalytical Ltd, Malvern WR14 1XZ, UK), meanwhile dynamic light scattering (DLS) was determined using a ZetaSizer Nano-ZS laser diffractometer (Malvern Panalytical Ltd, Malvern WR14 1XZ, UK) working at 633 nm and equipped with a backscatter detector [29]. Each nanoparticle sample was loaded into a disposable micro cuvette, before diluting with two mL of water. After that, the samples were sonicated for another 5 min and measured at 25 °C. Samples were also analyzed to determine their polydispersibility index, and their pH value using a pH meter (Adwa, AD8000, 6726 Szeged - Hungary)

2.5.3. Encapsulation efficiency

The chitosan nanoparticles loaded with *L. rhamnosus* bioactive metabolites were sealed in a 25 mL cylinder and stored at 25 °C for 24, 48, 72, and 96 h for the determination of encapsulation efficiency [30]. The percentage of encapsulation efficiency was calculated using Equation (1).

$$\text{Encapsulation efficiency } \% = \frac{VT - VS}{VT} \times 100 \quad (1)$$

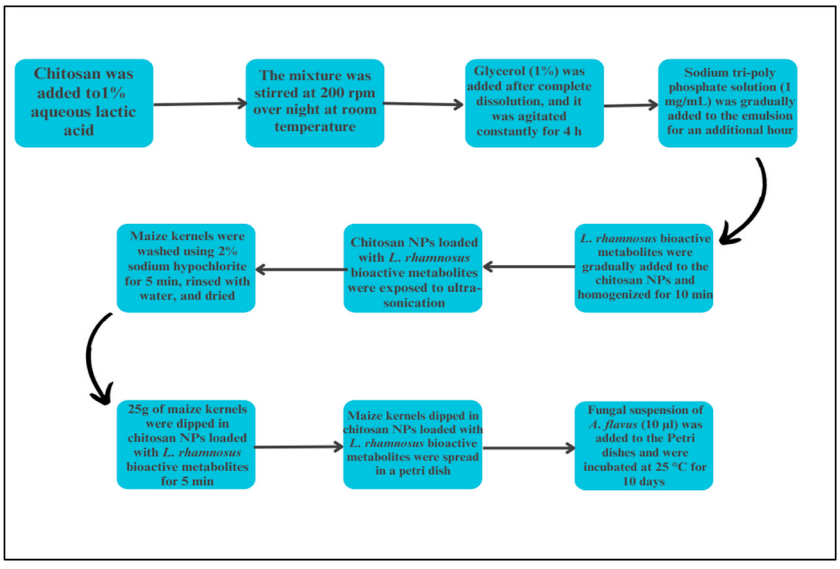

Figure (1). A process diagram showing the preparation of chitosan nanoparticles loaded with *L. rhamnosus* bioactive metabolites, as well as the dipping of maize kernels in chitosan nanoparticles loaded with *L. rhamnosus* bioactive metabolites.

Whereas VT: is the total volume of nanoparticles and VS: is the separated solution volume.

2.5.4. Fourier Transform Infrared Spectroscopy (FTIR)

Fourier Transform Infrared Spectroscopy analysis was conducted using JASCO FT/IR 4100, Yorkshire WF16 0 PR, UK fitted with a multi-zone nitrogen purge. Spectra were collected in the range of 4000 to 400 cm^{-1} with a resolution of 4 cm^{-1} [31]. The FTIR spectrometer was purged to reduce spectrum contributions. The mean of four spectra from different nanoparticles of the same sample was then computed.

2.6. Antifungal activity using agar well diffusion method

Radial growth measurement is a standard way to examine the development of filamentous fungus on a solid medium. It gives useful information regarding the growth of fungal colonies, therefore, the antifungal activity of chitosan nanoparticles loaded with different concentrations of *L. rhamnosus* bioactive metabolites was determined using the agar well diffusion technique. *Aspergillus flavus* spore suspension (10 μl, 10^3 spores/mL) spores/mL), was dissolved in sterile saline with 0.1 % (v/v) Tween 80 and counted using a hemocytometer. Fungal spores were inoculated onto the middle of a PDA plate. Wells were prepared using a cork borer around the primary inoculation point, and chitosan nanoparticles loaded with different concentrations of *L. rhamnosus* bioactive metabolites were administered to them. Plates were incubated at 28 °C for 5 days. The colony radial diameter was measured after 5 days of incubation.

2.7. Evaluation of A. flavus spore germination

The capacity of *A. flavus* to germinate in the presence of chitosan nanoparticles and chitosan nanoparticles loaded with *L. rhamnosus* bioactive metabolites was assessed [32] In multiwell plates, each well-received 200 μL of chitosan nanoparticles and *A. flavus* spore suspension (10 μL, 10^5 spores/mL). As a control, the fungus was put into sterile water. The plates were incubated at 25 °C in the dark and under aerobic circumstances. After 24 h, 20 μL of each solution was added to microscopic slides. The samples were examined using an optical microscope (Olympus, Tokyo, Japan). The percentage of germination inhibition rate (GIR%) was calculated using Equation (2).

$$\text{GIR } \% = \frac{\text{No. of germinated conidia in control} - \text{No. of germinated conidia in experimental}}{\text{No.of germinated conidia in control}} \times 100 \quad (2)$$

2.8. Evaluation of A. flavus spore viability

Chitosan nanoparticles and chitosan nanoparticles loaded with *L. rhamnosus* bioactive metabolites were introduced to a 50 mL Elemenyer flask containing yeast extract sucrose medium (YES, 20 g/L yeast extract, and 20 g/L sucrose). A suspension of *A. favus* spores (10^3 spores/mL) was added to a liquid medium and cultured for 24 h. As a control, the fungus was put into sterile water. During 24 h of incubation samples were taken every 6 h to perform a serial dilution (10^{-1} to 10^{-6}), which was spread onto PDA plates. Plates were incubated at 25 °C for 48 h. Fungal colonies were counted and expressed as CFU/mL, later, findings were expressed as log CFU/mL using Equation (3).

$$\text{logCFU} \,/\, \text{mL} = \log_{10} (\text{CFU} / \text{mL}) \quad (3)$$

The viability percentage was calculated using Equation (4).

$$\text{Viability percentage } \% = \frac{\text{logCFU} / \text{mL of experimental}}{\text{log CFU} / \text{mL of control}} \times 100 \quad (4)$$

2.9. Bio-control of maize kernels

With modifications, the bio-control of maize kernels against fungal growth was carried out following the method described by Muhialdin et al. [33]. Maize kernels were obtained from a retailer in Dokki, Giza, Egypt. Fresh maize kernels were washed using 2 % sodium hypochlorite for 5 min and rinsed well with sterilized distilled water. The maize was blotted dry between sterile Whatman No. 1 filter papers.

The maize kernels (25 g) were then transferred to sterile Petri dishes, whereas chitosan nanoparticles (10 mL) and chitosan nanoparticles loaded with *L. rhamnosus* bioactive metabolites (10 mL) were placed on them for 5 min to ensure uniform coating over the grains. Later, a fungal suspension of *A. flavus* (10 μl, 10^6 spores/mL) was added to the Petri dishes (Fig. 1) and then incubated at 25 °C for 10 days. Control was prepared of maize kernels not coated by chitosan nanoparticles. Blank was also prepared of maize kernels coated by chitosan nanoparticles only without the bioactive metabolites.

2.10. Fungal observation

The presence of fungal growth was observed in the Petri dishes containing maize kernels coated or not coated with chitosan nanoparticles loaded with *L. rhamnosus* bioactive metabolites after 3–10 days of storage at 25 °C.

2.11. Fungal count

After 10 days of storage at 25 °C, 10 g of each maize sample coated or not coated with chitosan nanoparticles loaded with *L. rhamnosus* bioactive metabolites were added to 90 mL of peptone water solution (0.1 % w/v). After 30 min of homogenization, the solution was decimally diluted (10^{-1} to 10^{-7}) before plating aliquots on the PDA medium. After incubation at 25 °C for 5 days, the colony forming units (CFU) were counted [34], and the findings were expressed as the number of CFU/g. Later, findings were expressed as log CFU/g.

The percentage of inhibition of fungal growth was calculated using Equation (5).

$$\text{Percentage of inhibition} = 1 - \frac{\text{CFU experimental}}{\text{CFU control}} \times 100 \tag{5}$$

Log reduction was also calculated using Equation (6).

$$\text{Log Reduction} = \text{Log CFU control} - \text{Log CFU experimental} \tag{6}$$

2.12. Statistical analysis

Results were expressed as mean ± SD. The statistical analysis was performed using the Microsoft Excel 2010 statistics program. Analysis of variance (ANOVA) was obtained, with $P < 0.05$ considered statistically significant.

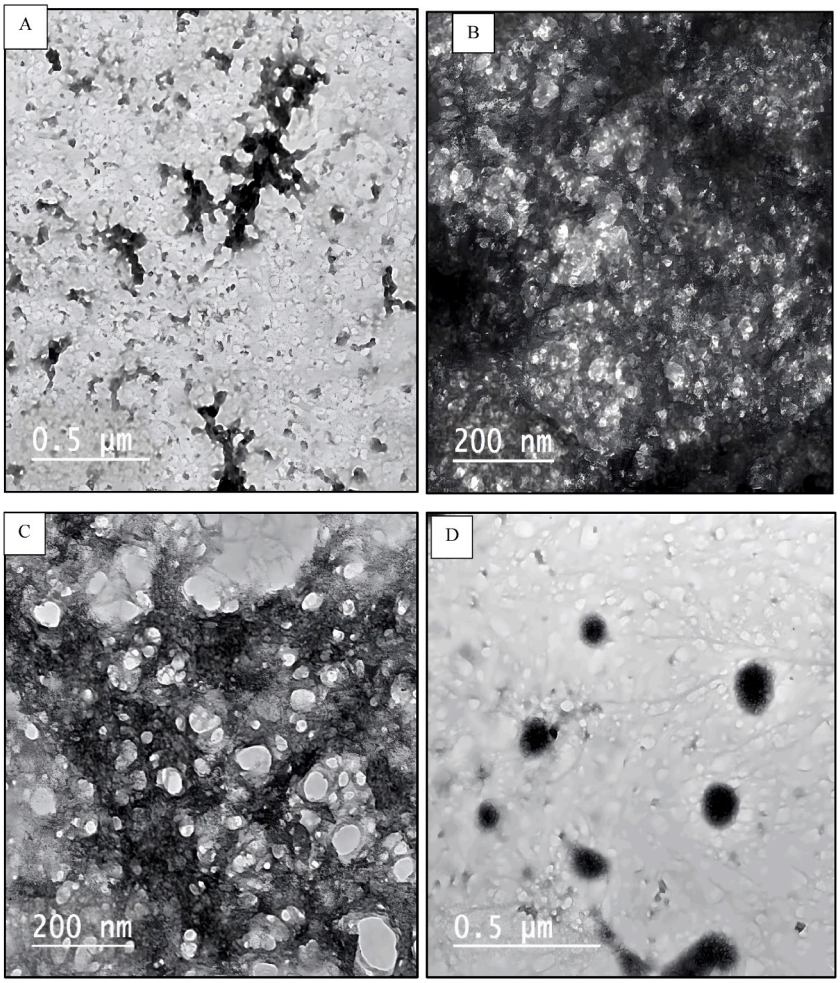

Figure (2). Transmission electron microscopic image of A) chitosan nanoparticles (blank); B) chitosan nanoparticles loaded with bioactive metabolites at 5 mg/mL concentration; C) chitosan nanoparticles loaded with bioactive metabolites at 7 mg/mL concentration; and D) chitosan nanoparticles loaded with bioactive metabolites at 9 mg/mL concentration.

3. Results and discussion

3.1. Transmission electron microscope

Transmission electron microscopy is another effective approach for determining the morphological structure of chitosan nanoparticles, and it was used at various magnification levels and can provide further data about particle aggregation and agglomeration. Results showed that the chitosan nanoparticles were spherical, had a smooth surface, and were different in nm diameter. Furthermore, the chitosan nanoparticles (blank) revealed a measurement range of 0.78–1.15 nm (Fig. 2A). The chitosan nanoparticles loaded with *L. rhamnosus* bioactive metabolites at a concentration of 5 mg/mL revealed a measurement range of 0.87–2.10 nm (Fig. 2B). Results also revealed that chitosan nanoparticles loaded with *L. rhamnosus* bioactive metabolites at a concentration of 7 mg/mL revealed a measurement range of 3.91–8.49 nm (Fig. 2C). Data also showed that the chitosan nanoparticles loaded with *L. rhamnosus* bioactive metabolites at a concentration of 9 mg/mL revealed a measurement range of 60–120 nm (Fig. 2D).

In our study, the size of chitosan nanoparticles was considered lower than those of Deng et al. [35] and higher than that of El-Naggar et al. [36]. The TEM images showed the physical aggregation of chitosan nanoparticles. This aggregation might be due to the small diameter of the particles or it could be due to the drying during TEM sample preparation [37].

3.2. Zeta potential, size distribution, and polydispersibility index

Results in Table (1) demonstrated that positively charged chitosan nanoparticles (blank) have a stable zeta potential of +41.1 ± 3.35 mV at 25 °C. The zeta potential showed a slight increase in their values with the increase in the concentration of *L. rhamnosus* bioactive metabolites in the chitosan nanoparticles to reach a zeta potential of +52.6 ± 3.75 mV. Additionally, the zeta potential distribution showed a single peak, thus showing the homogeneity of chitosan nanoparticles.

Several researchers reported that a stabilized nanoparticle suspension requires a zeta potential of a minimum of ±30 mV [38,39]. In our study, the zeta potential of chitosan nanoparticles ranged from +41.1 to +52.6 mV. In agreement, Qi et al. [40] showed that the surfaces of chitosan nanoparticles and copper-loaded nanoparticles exhibited a positive charge of approximately 51 mV. It was observed that the zeta potential showed a slight increase in their values with the increase in the amount of bioactive metabolite concentration in the nanoparticles. Thus, we could conclude that the greater the absolute value of the nanospheres' zeta potential, the greater the charge quantity on their surface. This could result in a more vital repelling interaction among the nanospheres and, therefore, higher stability and more uniform size of the nanoparticles [41].

The chitosan nanoparticles (blank) were measured to have a mean particle size of 63.1 ± 13.87 nm (Table 1). The particle size showed an increase in their values with the increase in the concentration of *L. rhamnosus* bioactive metabolites in the chitosan nanoparticles to reach a mean particle size of 175.1 ± 51.67 nm. It was observed that the particle sizes determined by the DLS instrument were larger than those observed by the TEM except for chitosan nanoparticles loaded with *L. rhamnosus* bioactive metabolites at a concentration of 9 mg/mL which was higher than the TEM (Fig. 2). The different measuring conditions; that is, the dry and hydrodynamic states, respectively, involved in both methods may be the cause of the size difference between TEM and DLS analysis [42]. In a different study, Qureshi et al. [43] reported that the size verified by DLS is supported by the size derived from the TEM.

The PDI was used to determine the average homogeneity of a nanoparticle, and can also reveal nanoparticle aggregation. Data in Table (1) demonstrated that the PDI of chitosan nanoparticles (blank) reached 0.501, and increased to reach 0.695 for chitosan nanoparticles loaded with *L. rhamnosus* bioactive metabolites at a concentration of 9 mg/mL The distribution of PDI values were considered very heterogeneous as they were more than 0.5 [44].

3.3. Encapsulation efficiency

The encapsulation efficiency of chitosan nanoparticles loaded with *L. rhamnosus* bioactive metabolites at a concentration of 5 mg/mL reached 98.3 ± 1.18 % (Table 1). It was observed that the encapsulation efficiency decreased by increasing the concentration of *L. rhamnosus* bioactive metabolites to 9 mg/mL in chitosan nanoparticles, the encapsulation efficiency reached 93.6 ± 1.88 %. The interactions between the polymers utilized as well as the active groups in the *L. rhamnosus* bioactive metabolites can have a considerable impact on nanoparticle encapsulation efficiency. These interactions, such as hydrogen bond formation, might influence the

Table (1)
Characteristics of chitosan nanoparticles.

Formula	Particle size (nm)	Zeta potential (mV)	PDI	pH	Encapsulation efficiency (%)
Blank CNP	63.1 ± 13.87	41.1 ± 3.35	0.501	7.93	–
CNPLR 5 mg/mL	63.6 ± 13.10	50.6 ± 3.39	0.627	5.51	98.3 ± 1.18
CNPLR 7 mg/mL	173.7 ± 57.37	51.3 ± 5.09	0.531	5.34	96.7 ± 1.54
CNPLR 9 mg/mL	175.1 ± 51.67	52.6 ± 3.75	0.695	5.26	93.6 ± 1.88

Results are mean ± SD ($n = 3$).
Blank CNP: Chitosan nanoparticles only.
CNPLR: Chitosan nanoparticle loaded with *L. rhamnosus* bioactive metabolites with different concentrations (5, 7, and 9 mg/mL).
Statistical analysis revealed no significant difference $P > 0.05$ between different formulas.

encapsulated material's stability and release qualities. Chitosan can considerably increase the stability of nanoparticles loaded with *L. rhamnosus* bioactive metabolites, as chitosan is noted for its good film-forming properties, which help in reducing creaming, a phenomenon in which the dispersed phase rises to the surface owing to density differences. This is especially useful for food preservation, where nanoparticle stability is critical.

3.4. Fourier Transform Infrared Spectroscopy

The FTIR analysis is a strong method for identifying functional groups. Data in Figure (3) and Table (2) illustrated the FTIR spectra of chitosan nanoparticles in the range of 4000-500 cm^{-1}, allowing the understanding of better functional groups' nature. FTIR spectra of chitosan nanoparticles (blank) had several peaks, the first at 661.46 cm^{-1} which represents C-H bending, alkynes. Bands appearing at, 1645.84, and 3356.60 cm^{-1} represented C=C stretching, alkene, and N-H stretching of aliphatic primary amine, respectively.

The FTIR spectra of the chitosan nanoparticles loaded with *L. rhamnosus* bioactive metabolites at a concentration of 5 mg/mL, indicated the presence of numerous peaks. The first band appeared at 619.04 cm^{-1} representing C-H, alkyne, followed by 1089.58 cm^{-1} indicating a C-O stretching. Bands appearing at 1328.71, 1525.42, 1629.55 and 3411.46 cm-^{1} represent C-N stretching, aromatic amines, N-O stretching, nitro compound, C=C stretching, alkene, and O-H stretching, and alcohol respectively.

The FTIR spectra of chitosan nanoparticles loaded with *L. rhamnosus* bioactive metabolites at a concentration of 7 mg/mL showed four bands appearing at 611.32, 1085.73, 1637.27, and 3369.03 cm^{-1} representing C-H bending, alkynes C-O stretching, alcohol, C=C stretching, alkene, N-H stretching, and aliphatic primary amine respectively.

The functional groups found in chitosan nanoparticles loaded with *L. rhamnosus* bioactive metabolites at a concentration of 9 mg/mL, indicated the presence of the following bands at 657.607, 1455.99, 1637.27 and 3365.17 cm^{-1} representing C-H bending for alkynes and alkanes, C=C stretching, alkene, and N-H stretching aliphatic primary amine respectively.

Similar results were reported by El-Naggar et al. [36] who indicated that the FTIR spectra of chitosan nanoparticles showed absorption bands at 3442, 1572, and 645 cm^{-1}. The absorption peaks in the range 900–1200 cm^{-1} are caused by the antisymmetric C-O stretching of chitosan's saccharide structure [45]. The peak at 3411 cm^{-1} is ascribed to O-H, stretching vibration, and intramolecular hydrogen bonding [46,47]. Chitosan spectra are known to have a distinctive wide band at 3411 cm^{-1} due to OH stretching vibrations [48,49]. Similar observations were reported by Pavinatto et al. [50] and Yadav & Yadav [28].

3.5. Antifungal activity

Results in Table (3) revealed that the radial growth diameter of *A. flavus* was recorded at 20.80 mm when adding chitosan nanoparticles only. It was observed that chitosan nanoparticles loaded by *L. rhamnosus* bioactive metabolites at concentrations 5 and 7 mg/mL reduced the radial growth diameter of *A. flavus* to 5.10 and 3.60 mm respectively. At a higher concentration of *L. rhamnosus* bioactive metabolites (9 mg/mL) radial growth diameter increased due to a paradoxical effect.

3.6. Germination and viability of A. flavus fungal spores

Table (4) displays the antifungal efficacy of chitosan nanoparticles (blank) and those containing *L. rhamnosus* bioactive metabolites against *A. flavus* spore germination. The acquired findings were compared to distilled water containing *A. flavus*. All formulations significantly suppressed spore germination compared to the control. Chitosan nanoparticles containing *L. rhamnosus* bioactive

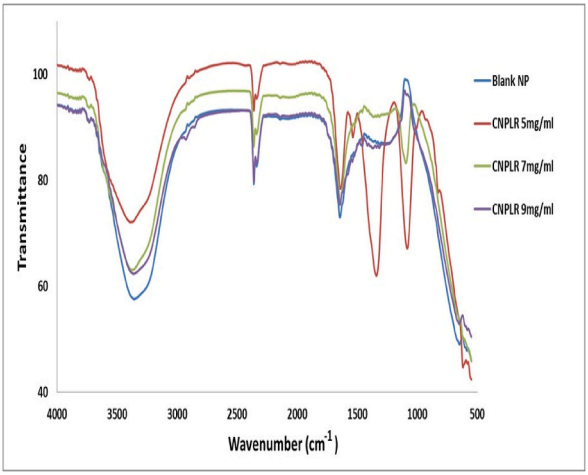

Figure (3). The FTIR spectra of chitosan nanoparticle; A) Blue: blank chitosan nanoparticles; B) Dark red: chitosan nanoparticle loaded with *L. rhamnosus* bioactive metabolites at a concentration of 5 mg/mL; C) Green: chitosan nanoparticle loaded with *L. rhamnosus* bioactive metabolites at a concentration of 7 mg/mL; and D) Purple: chitosan nanoparticle loaded with *L. rhamnosus* bioactive metabolites at a concentration of 9 mg/mL.

Table (2)
The FTIR spectra of different formulas of chitosan nanoparticles.

IR frequencies (cm^{-1})				Functional groups
Blank CNPs	CNPLR 5 mg/mL	CNPLR 7 mg/mL	CNPLR 9 mg/mL	
661.46	619.04	611.32	657.607	**Alkynes (C-H bend)**
–	1089.58	1085.73	–	**Alcohol (C-O stretch)**
–	–	–	1455.99	**Alkane (C-H bend)**
–	1328.71	–	–	**Aromatic amine (C-N stretch)**
–	1525.42	–	–	**Nitro compound (N-O stretch)**
1648.84	1629.55	1637.27	1637.27	**Alkene (C=C stretch)**
–	3411.46	–	–	**Alcohol (O-H stretch)**
3356.60	–	3369.03	3365.17	**Aliphatic primary amine (N-H stretch)**

Blank CNP: Chitosan nanoparticles only.
CNPLR: Chitosan nanoparticle loaded with *L. rhamnosus* bioactive metabolites with different concentrations (5, 7, and 9 mg/mL).

Table (3)
Effect of different formulas of chitosan nanoparticles on *A. flavus* radial growth diameter.

Formula	Radial growth diameter (mm)	Inhibition diameter (mm)	Percentage of inhibition of radial growth diameter (%)
Blank CNP	20.80 ± 0.59	–	–
CNPLR 5 mg/mL	5.10 ± 0.28	15.70	75.48 %
CNPLR 7 mg/mL	3.60 ± 0.34	17.20	82.69 %
CNPLR 9 mg/mL	5.60 ± 0.75	15.20	73.8 %

Results are mean ± SD ($n = 3$).
Blank CNP: Chitosan nanoparticles only.
CNPLR: Chitosan nanoparticle loaded with *L. rhamnosus* bioactive metabolites with different concentrations (5, 7, and 9 mg/mL).
Results revealed a significant difference $P < 0.05$ between the different formulas.

metabolites at a concentration of 7 mg/mL inhibited spore germination most effectively (89.87 %), while the lowest inhibition percentage was found at a concentration of 9 mg/mL (67.09 %). Meanwhile, blank chitosan nanoparticles reduced *A. flavus* spore germination by 34.77 %.

An *in vitro* investigation of *Penicillium expansum* and *Botrytis cinerea* treated with chitosan revealed that *P. expansum* had higher spore germination inhibition than *B. cinerea* [51]. It was noted that chitosan affected the germination of *Alternaria alternata* spores [52]. The administration of chitosan and carvacrol in combination significantly impeded *A. flavus* mycelial development and spore germination [53]. The compounds tested affected the cell wall, modifying its composition, preventing its development, causing cell death, and lowering spore germination [54].

The antifungal efficacy of chitosan nanoparticles (blank) and those containing *L. rhamnosus* bioactive metabolites on the viability of *A. flavus* spores was shown in Table (4). Data clearly showed that chitosan nanoparticles greatly affect the viability percentage of fungal spores during 24h. At the end of the incubation period chitosan nanoparticles containing *L. rhamnosus* bioactive metabolites at concentrations of 5 and 7 mg/mL reduced spore viability percentage by 75.00 and 76.85 % respectively. Meanwhile, chitosan nanoparticles containing *L. rhamnosus* bioactive metabolites at a concentration of 9 mg/mL reduced spore viability percentage by 65.74 %. It was observed that a higher effect on spore viability was for chitosan nanoparticles loaded by *L. rhamnosus* bioactive metabolites compared to chitosan nanoparticles alone.

Luque-Alcaraz et al. [55], examined the impact on the viability of *A. parasiticus* spores of various concentrations of chitosan nanoparticle-encapsulating pepper tree essential oils. When compared to the control, it was discovered that all formulas decreased the vitality of fungal spores. It was noted that when the dose of nickel chitosan nanoparticles increased, the spore viability percentage was reduced [56]. The results were significantly confirmed by the outcomes obtained by Ghasemian et al. [57], who said that metallic

Table (4)
Effect of different formulas of chitosan nanoparticles on the germination inhibition rate (GIR %) and viability of *A. flavus* fungal spores.

Formula	GIR (%)	Time (hours)				
		0 h	6 h	12 h	18 h	24 h
Blank CNP	34.77 ± 1.41	100 ± 0.00	92.22 ± 3.64	83.12 ± 3.32	72.29 ± 4.26	62.04 ± 0.91
CNPLR 5 mg/mL	83.54 ± 1.29	100 ± 0.00	93.61 ± 5.31	84.4 ± 2.93	79.04 ± 2.30	75.00 ± 5.00
CNPLR 7 mg/mL	89.87 ± 0.82	100 ± 0.00	95.28 ± 3.32	86.19 ± 3.77	80.48 ± 1.86	76.85 ± 1.85
CNPLR 9 mg/mL	67.09 ± 5.72	100 ± 0.00	94.44 ± 2.00	83.38 ± 1.62	72.77 ± 2.85	65.74 ± 2.76

Results are mean ± SD ($n = 3$).
Blank CNP: Chitosan nanoparticles only.
CNPLR: Chitosan nanoparticle loaded with *L. rhamnosus* bioactive metabolites with different concentrations (5, 7, and 9 mg/mL).
Results revealed a significant difference of $P < 0.05$ between the different formulas and no significant difference of $P > 0.05$ between times.

nanoparticles are beneficial in lowering spore viability percentage, notably for *Fusarium solani.*

3.7. Fungal observation

In addition to assessing the qualitative and quantitative antifungal activity of chitosan nanoparticles loaded with *L. rhamnosus* bioactive metabolites, the potential to extend the shelf life of maize kernels was studied (Table 5). The first appearance of visible fungal growth defined the shelf life. Under similar storage conditions, the fungal development of the control and chitosan blank groups was observed on maize kernels after three days. Similarly, maize kernels sprayed by chitosan nanoparticles loaded with *L. rhamnosus* bioactive metabolites at concentrations of 5 and 9 mg/mL A. *flavus* was observed on maize kernels after three days. On the other hand, chitosan nanoparticles loaded with *L. rhamnosus* bioactive metabolites at a concentration of 7 mg/mL prevented fungal growth for 10 days.

3.8. Fungal count

The effects of coating maize kernels with chitosan nanoparticles and chitosan nanoparticles loaded with different doses of *L. rhamnosus* bioactive metabolites on *A. flavus* count were investigated after 10 days of storage (Fig. 4, Table 6). Data in Figure (4) depicts the beneficial effects of maize kernels treated with chitosan nanoparticles containing *L. rhamnosus* bioactive metabolites on the growth of *A. flavus*. After 10 days of storage, non-coated maize kernels were fully covered with *A. flavus* (Fig. 4A). Maize kernels coated with chitosan nanoparticles only slightly reduced the fungal growth (Fig. 4B). On the other hand, coating maize kernels with chitosan nanoparticles containing *L. rhamnosus* bioactive metabolites at a concentration of 5, and 9 mg/mL reduced the *A. flavus* mold decay to a minimum (Fig. 4C, D), whereas maize kernels treated with chitosan nanoparticle containing *L. rhamnosus* bioactive metabolites at a concentration of 7 mg/mL completely prevented fungal growth (Fig. 4E). It could be concluded that by preventing fungal growth, mycotoxin production was prevented.

In a similar study, Martínez-Batista et al. [58] revealed that chitosan effectively inhibited *A. niger*, *P. funiculosum*, and *F. verticillioides* in preserved maize kernels. Citrus fruit treated by chitosan nanoparticle at a concentration of 250 ppm prevented the growth of *Lasiodiplodia pseudotheobromae*, *Alternaria alternate*, and *Penicillium digitatum*, whereas no blight and rot symptoms were observed [59].

Results in Table (4) showed that non-coated maize kernels had a high growth rate with a final fungal count of 3.22 log CFU/g. Maize kernels coated with chitosan nanoparticles only had considerably low fungal counts with values of 2.65 log CFU/g. On the other hand, coating maize kernels with chitosan nanoparticles containing *L. rhamnosus* bioactive metabolites at a concentration of 5, and 9 mg/mL reduced fungal count to 2.62, and 3.02 log CFU/g respectively. Meanwhile, maize kernels treated with chitosan nanoparticles containing *L. rhamnosus* bioactive metabolites at a concentration of 7 mg/mL effectively reduced the fungal count to 2.23 log CFU/g. The percentage of inhibition for the fungal count was calculated and found to be 73.41 %, 89.42 %, and 39.06 % for maize kernels coated with chitosan nanoparticles containing *L. rhamnosus* bioactive metabolites at concentrations of 5, 7, and 9 mg/mL, respectively.

It was observed that by increasing the concentration of *L. rhamnosus* bioactive metabolites to 9 mg/mL in chitosan nanoparticles, fungal growth resumed. This is called the paradoxical effect, which is a well-known phenomenon in the use of antifungal agents against pathogenic fungi, notably those from the *Candida* and *Aspergillus* genera [60,61], indicating that antifungals at high concentrations have the opposite effect, reactivating or increasing the expression of particular genes, which is thought to be a type of fungus defense mechanism.

On the other hand, it was noted that chitosan nanoparticles containing *L. rhamnosus* bioactive metabolites at a concentration of 5, and 7 mg/mL effectively decreased fungal growth. This could be due to the presence of chitosan which is known to be effective in inhibiting the growth of pathogenic fungi [62,63]. Several mechanisms have been postulated to explain the antifungal activity of chitosan, and these include local disintegration of fungal cell membranes, leaking of cytoplasm, chelation of essential nutrients, and binding of nucleic acids that disrupt the flow of genetic information [13,64].

Furthermore, the antifungal activity of chitosan nanoparticles containing *L. rhamnosus* bioactive metabolites could be due to the presence of bioactive metabolites such as volatile organic compounds, organic acids, and polyphenols [25]. The volatile organic

Table (5)
Monitoring of fungal growth on maize kernels contaminated with *Aspergillus flavus* during 10 days of storage.

Formula	Days			
	0	3	7	10
Control	–	+	+	+
Blank CNP	–	+	+	+
CNPLR 5 mg/mL	–	+	+	+
CNPLR 7 mg/mL	–	–	–	–
CNPLR 9 mg/mL	–	+	+	+

Control: No chitosan nanoparticles were added to the maize kernels.
Blank CNP: Chitosan nanoparticles only.
CNPLR: Chitosan nanoparticle loaded with *L. rhamnosus* bioactive metabolites with different concentrations (5, 7, and 9 mg/mL).
Fungal growth is expressed as (+), and the absence of fungal growth is described as (−).

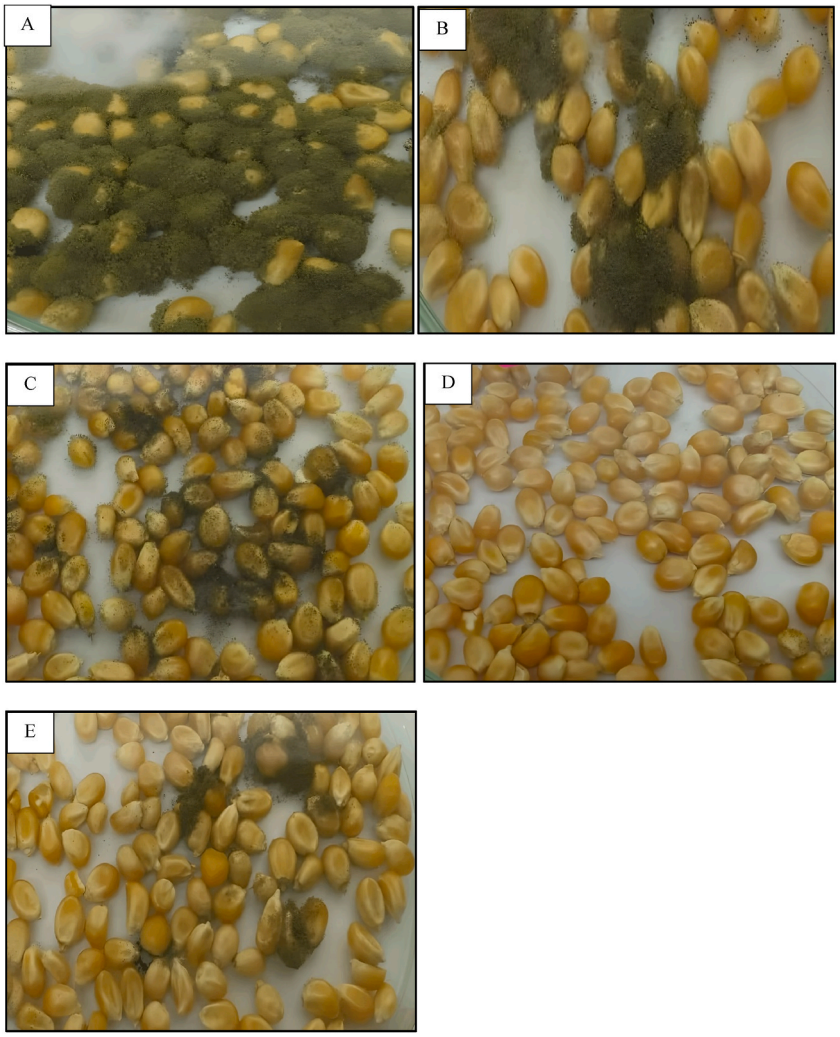

Figure (4). Inhibition of *A. flavus* growth by chitosan nanoparticles loaded with *L. rhamnosus* bioactive metabolites on the surface of maize kernels, A) maize kernels with no chitosan nanoparticles, B) maize kernels with chitosan nanoparticles and no bioactive metabolites, C) maize kernels with chitosan nanoparticles loaded with *L. rhamnosus* bioactive metabolites at a concentration of 5 mg/mL, D) maize kernels with chitosan nanoparticles loaded with *L. rhamnosus* bioactive metabolites at a concentration of 7 mg/mL, E) maize kernels with chitosan nanoparticles loaded with *L. rhamnosus* bioactive metabolites at a concentration of 9 mg/mL.

Table (6)
Total fungal count (log CFU/g) in maize kernels treated by different formulas of chitosan nanoparticles after 10 days of storage.

Formula	Log CFU/g	Log reduction	Percentage of inhibition (%)
Control	3.22 ± 0.04	–	–
Blank CNP	2.65 ± 0.16	0.57	72.91 %
CNPLR 5 mg/mL	2.62 ± 0.08	0.60	73.41 %
CNPLR 7 mg/mL	2.23 ± 0.20	0.99	89.42 %
CNPLR 9 mg/mL	3.02 ± 0.21	0.20	36.09 %

Results are mean ± SD ($n = 3$).
Control: No chitosan nanoparticles were added to the maize kernels.
Blank CNP: Chitosan nanoparticles only.
CNPLR: Chitosan nanoparticle loaded with *L. rhamnosus* bioactive metabolites with different concentrations (5, 7, and 9 mg/mL).
Results revealed a significant difference $P < 0.05$ between the different formulas.

compound 9, 12-octadecadienoic acid (Z, Z) extracted from several lactic acid bacteria was found to have antifungal activity [65,66]. Several investigations showed that organic acids including acetic acid, lactic acid, and phenyl lactic acid have a substantial role in antifungal activity [67,68]. Organic acids such as citric and lactic acids may inhibit fungal growth by changing membrane structure, lowering intracellular pH, inhibiting active transport, and interfering with metabolic processes [63]. Recently, significant antifungal efficacy against *P. digitatum* was exhibited by polyphenols [64]. The mechanism underlying polyphenols' antifungal activity involves the pathogenic microorganism's cell wall and membrane being penetrated and disrupted. This, in turn, interferes with critical processes like electron transfer, information transfer, nucleotide synthesis, and other internal and external activities of the microorganism [65].

Incorporating bioactive metabolites into a biodegradable coating base to give antifungal characteristics is a common strategy, whereas this technique showed promise for creating edible films and coatings with antifungal characteristics, which may be employed for food packaging. Natural extracts are considered safer for humans and the environment compared to nano-antibacterial agents made from inorganic materials [69]. Chitosan edible films often contain antimicrobial agents such as essential oils [70], plant extracts [71], and bacteriocins [72].

It could be concluded that chitosan nanoparticles have antifungal capabilities that can impede the growth and metabolic activities of *A. flavus* and may potentially lower mycotoxin levels. The combined action of chitosan nanoparticles and *L. rhamnosus* bioactive metabolites can result in synergistic antifungal activity, greatly reducing *A. flavus*, whereas reduced fungal biomass may correlate with lower mycotoxin production.

This study is one of the rare attempts to combine chitosan nanoparticles with bacterial bioactive metabolites, as this innovative combination has the potential to synergistically improve the antifungal capabilities of the chitosan nanoparticles, giving a fresh strategy for fighting fungal contamination. Although chitosan nanoparticles and bacterial metabolites have been researched separately for their antimicrobial characteristics, their combination in the context of antifungal activity is a relatively new topic of research. The possible synergistic effects of these components gave information on their combined efficacy against fungal contamination.

The limitation identified in this study is the possibility that high concentrations of bioactive metabolites produce a paradoxical effect, which underlines an essential concern in the design and interpretation of studies using chitosan and antifungal drugs. As a result, it is critical to determine the appropriate dosage of chitosan and antifungal agents to achieve the intended outcome while minimizing any side effects.

4. Conclusion

This study is built on our previous findings, which revealed that the bioactive metabolites extracted from *L. rhamnosus* comprised organic acids, volatile organic compounds, and polyphenols, and exhibited antifungal and antiaflatoxigenic properties. The characterization of synthesized chitosan nanoparticles showed that the size ranged from 63.1 to 175.1 nm, whereas zeta potential varied from 41.1 to 52.6 mV. The encapsulation efficiency ranged from 93.6 to 98.3 %. The incorporation of *Lactobacillus rhamnosus* bioactive metabolites in chitosan nanoparticles offered a unique and effective technique for affecting the germination and viability of fungal spores and preventing *A. flavus* growth on grains. The effects of chitosan nanoparticles containing *Lactobacillus rhamnosus* bioactive metabolites resulted in a robust antifungal system with potential uses in food safety.

CRediT authorship contribution statement

Aya Abdel-Nasser: Writing – original draft, Methodology. **Hayam M. Fathy:** Supervision. **Ahmed N. Badr:** Supervision, Methodology. **Olfat S. Barakat:** Writing – review & editing, Supervision. **Amal S. Hathout:** Writing – review & editing, Supervision, Methodology.

Ethical statement

Not applicable.

Data availability statement

Data will be made available on request from the corresponding author.

Declaration of competing interest

The authors declare that they have no known competing financial interests or personal relationships that could have appeared to influence the work reported in this paper.

References

[1] H. Shi, J. Li, Y. Zhao, J. Mao, H. Wang, J. Zhu, Effect of *Aspergillus flavus* contamination on the fungal community succession, mycotoxin production and storage quality of maize kernels at various temperatures, Food Res. Int. 174 (2) (2023) 113662.
[2] O. Pechanova, T. Pechan, Maize-pathogen interactions: an ongoing combat from a proteomics perspective, Int. J. Mol. Sci. 16 (12) (2015) 28429–28448.

[3] A. Tarazona, J.V. Gómez, F. Mateo, M. Jiménez, D. Romera, E.M. Mateo, Study on mycotoxin contamination of maize kernels in Spain, Food Control 118 (2020) 107370.
[4] M. Carvajal-Moreno, Mycotoxin challenges in maize production and possible control methods in the 21st century, J. Cereal. Sci. 103 (2022) 103293.
[5] Q.N. Nji, O.O. Babalola, M. Mwanza, Aflatoxins in maize: can their occurrence Be effectively managed in africa in the face of climate change and food insecurity? Toxins 14 (8) (2022) 574.
[6] R.O.J.H. Stutt, M.D. Castle, P. Markwell, R. Baker, C.A. Gilligan, An integrated model for pre- and post-harvest aflatoxin contamination in maize, Sci. Food 7 (1) (2023) 1–15.
[7] S.K. Pankaj, H. Shi, K.M. Keener, A review of novel physical and chemical decontamination technologies for aflatoxin in food, Trends Food Sci. Technol. 71 (2018) 73–83.
[8] V. Ostry, F. Malir, J. Toman, Y. Grosse, Mycotoxins as human carcinogens—the IARC Monographs classification, Mycotoxin Res. 33 (1) (2017) 65–73.
[9] A. Kowalska, K. Walkiewicz, P. Kozieł, M. Muc-Wierzgoń, Aflatoxins: characteristics and impact on human health, Postep. Hig Med Dosw 71 (2017) 315–327.
[10] H. Li, et al., Early detection and monitoring for *Aspergillus flavus* contamination in maize kernels, Food Control 121 (2021) 107636.
[11] S.H. Nile, V. Baskar, D. Selvaraj, A. Nile, J. Xiao, G. Kai, in: Nanotechnologies in Food Science: Applications, Recent Trends, and Future Perspectives, vol. 12, Springer, Singapore, 2020, 1.
[12] N.E.A. El-Naggar, W.E.I.A. Saber, A.M. Zweil, S.I. Bashir, An innovative green synthesis approach of chitosan nanoparticles and their inhibitory activity against phytopathogenic *Botrytis cinerea* on strawberry leaves, Sci. Rep. 12 (1) (2022) 1–20.
[13] A. Kheiri, S.A.M. Jorf, A. Malihipour, H. Saremi, M. Nikkhah, Application of chitosan and chitosan nanoparticles for the control of Fusarium head blight of wheat (*Fusarium graminearum) in vitro* and greenhouse, Int. J. Biol. Macromol. 93 (A) (2016) 1261–1272.
[14] K. Divya, V. Smitha, M.S. Jisha, Antifungal, antioxidant and cytotoxic activities of chitosan nanoparticles and its use as an edible coating on vegetables, Int. J. Biol. Macromol. 114 (2018) 572–577.
[15] J. Yu, D. Wang, N. Geetha, K.M. Khawar, S. Jogaiah, M. Mujtaba, Current trends and challenges in the synthesis and applications of chitosan-based nanocomposites for plants: a review, Carbohydr. Polym. 261 (2021) 117904.
[16] I. Koumentakou, A. Meretoudi, C. Emmanouil, G.Z. Kyzas, Environmental toxicity and biodegradation of chitosan derivatives: a comprehensive review, J. Ind. Eng. Chem. (2024). Press.
[17] A. Farouk, A.S. Hathout, M.M. Amer, O.A. Hussain, A.S.M. Fouzy, The impact of nanoencapsulation on volatile constituents of *Citrus sinesis* L. Essential oil and their antifungal activity, Egypt. J. Chem. 65 (3) (2022) 519–530.
[18] J.P. Gh, et al., An overview on smart and active edible coatings: safety and regulations, Eur. Food Res. Technol. 249 (2023) 1935–1952.
[19] N. Muñoz-Tebar, J.A. Pérez-Álvarez, J. Fernández-López, M. Viuda-Martos, Chitosan edible films and coatings with added bioactive compounds: antibacterial and antioxidant properties and their application to food products: a review, Polymers 15 (2) (2023).
[20] O. Cota-Arriola, M.O. Cortez-Rocha, E.C. Rosas-Burgos, A. Burgos-Hernández, Y.L. López-Franco, M. Plascencia-Jatomea, Antifungal effect of chitosan on the growth of *Aspergillus parasiticus* and production of aflatoxin B_1, Polym. Int. 60 (6) (2011) 937–944.
[21] J.F.M. da Silva, et al., Utilização de filme de quitosana para o controle de aflatoxinas em amendoim, Bragantia, Campinas 74 (4) (2015) 467–475.
[22] C. Gupta, Natural useful therapeutic products from microbes, J. Microbiol. Exp. 1 (1) (2014) 30–37.
[23] V. Singh, Microbial bioactive components: sources, applications, and sustainability, in: M. Thakur, T. Belwal (Eds.), Bioactive Components A Sustainable System for Good Health and Well-Being, Springer, 2022, pp. 103–120.
[24] N.A. Al-Tayyar, A.M. Youssef, R.R. Al-Hindi, Edible coatings and antimicrobial nanoemulsions for enhancing shelf life and reducing foodborne pathogens of fruits and vegetables: a review, Sustain. Mater. Technol. 26 (2020) e00215.
[25] A. Abdel-Nasser, A.S. Hathout, A.N. Badr, O.S. Barakat, H.M. Fathy, Extraction and characterization of bioactive secondary metabolites from lactic acid bacteria and evaluating their antifungal and antiaflatoxigenic activity, Biotechnol. Reports 38 (2023) e00799.
[26] A. Abdel-Nasser, H.M. Fathy, A.N. Badr, A.S. Hathout, O.S.M. Barakat, Prevalence of aflatoxigenic fungi in cereal grains and their related chemical metabolites, Egypt. J. Chem. 65 (10) (2022) 455–470.
[27] M.J.N. Rajaofera, et al., Volatile organic compounds of *Bacillus atrophaeus* HAB-5 inhibit the growth of *Colletotrichum gloeosporioides*, Pestic. Biochem. Physiol. 156 (February) (2019) 170–176.
[28] P. Yadav, A.B. Yadav, Preparation and characterization of BSA as a model protein loaded chitosan nanoparticles for the development of protein-/peptide-based drug delivery system, Futur. J. Pharm. Sci. 7 (1) (2021).
[29] A. Farouk, A.N. Badr, A.S. Hathout, T.A. Morsy, A.S.M. Fouzy, G.N. Abdel-Rahman, Pomegranate peel nanoemulsion: evaluation of bioactive components and their efficacy to reduce specific pesticide residues, Egypt. J. Chem. 66 (13) (2023) 1433–1448.
[30] B.A. Sabry, A.N. Badr, K.A. Ahmed, M.A. Desoukey, D.M. Mohammed, Utilizing lemon peel extract and its nano-emulsion to control aflatoxin toxicity in rats, Food Biosci. 50 (PA) (2022) 101998.
[31] O.A. Hussain, E.A. Abdel Rahim, A.N. Badr, A.S. Hathout, M.M. Rashed, A.S.M. Fouzy, Total phenolics, flavonoids, and antioxidant activity of agricultural wastes, and their ability to remove some pesticide residues, Toxicol. Reports 9 (February) (2022) 628–635.
[32] I. Muzzalupo, G. Badolati, A. Chiappetta, N. Picci, R. Muzzalupo, *In vitro* antifungal activity of olive (*Olea europaea*) leaf extracts loaded in chitosan nanoparticles, Front. Bioeng. Biotechnol. 8 (March) (2020) 1–10.
[33] B.J. Muhialdin, et al., Antifungal activity determination for the peptides generated by *Lactobacillus plantarum* TE10 against *Aspergillus flavus* in maize seeds, Food Control 109 (2020) 106898.
[34] M.F.P. De Castro, N. Bragagnolo, S.R. Valentini, The relationship between fungi growth and aflatoxin production with ergosterol content of corn grains, Brazilian J. Microbiol. 33 (1) (2002) 22–26.
[35] Q.Y. Deng, C.R. Zhou, B.H. Luo, Preparation and characterization of chitosan nanoparticles containing lysozyme, Pharm. Biol. 44 (5) (2006) 336–342.
[36] N.E.A. El-Naggar, A.M. Shiha, H. Mahrous, A.B.A. Mohammed, Green synthesis of chitosan nanoparticles, optimization, characterization and antibacterial efficacy against multi-drug resistant biofilm-forming *Acinetobacter baumannii*, Sci. Rep. 12 (1) (2022) 1–19.
[37] A. Ghadi, S. Mahjoub, F. Tabandeh, F. Talebnia, Synthesis and optimization of chitosan nanoparticles: potential applications in nanomedicine and biomedical engineering, Casp. J. Intern. Med. 5 (3) (2014) 156–161.
[38] N.M. Zain, A.G.F. Stapley, G. Shama, Green synthesis of silver and copper nanoparticles using ascorbic acid and chitosan for antimicrobial applications, Carbohydr. Polym. 112 (2014) 195–202.
[39] A. Manikandan, M. Sathiyabama, Green synthesis of copper-chitosan nanoparticles and study of its antibacterial activity, J. Nanomed. Nanotechnol. 6 (1) (2015) 100025.
[40] L. Qi, Z. Xu, X. Jiang, C. Hu, X. Zou, Preparation and antibacterial activity of chitosan nanoparticles, Carbohydr. Res. 339 (16) (2004) 2693–2700.
[41] A.J. Wan, Y. Sun, W.T. Li, H.L. Li, Transmission electron microscopy and electron diffraction study of BSA-loaded quaternized chitosan nanoparticles, Journal of Biomedical Materials Research - Part B Applied Biomaterials 86 (1) (2008) 197–207.
[42] M. Sathiyabama, et al., Green synthesis of chitosan nanoparticles using tea extract and its antimicrobial activity against economically important phytopathogens of rice, Sci. Rep. 14 (1) (2024) 1–10.
[43] W.A. Qureshi, B. Vivekanandan, J.A. Jayaprasath, D. Ali, S. Alarifi, K. Deshmukh, Antimicrobial activity and characterization of pomegranate peel-based carbon dots, J. Nanomater. 2021 (2021).
[44] A. Bayat, B. Larijani, S. Ahmadian, H.E. Junginger, M. Rafiee-Tehrani, Preparation and characterization of insulin nanoparticles using chitosan and its quaternized derivatives, Nanomedicine Nanotechnology, Biol. Med. 4 (2) (2008) 115–120.
[45] A. Laaraibi, et al., Chitosan-Clay Based (CS-NaBNT) Biodegradable Nanocomposite Films for Potential Utility in Food and Environment, Intech Open, 2018.
[46] J. Kumirska, et al., Application of spectroscopic methods for structural analysis of chitin and chitosan, Mar. Drugs 8 (5) (2010) 1567–1636.
[47] F. Damiri, Y. Bachra, C. Bounacir, A. Laaraibi, M. Berrada, Synthesis and characterization of lyophilized chitosan-based hydrogels cross-linked with benzaldehyde for controlled drug release, J. Chem. 2020 (2020).

[48] C. Rodrigues, et al., Mechanical, thermal and antimicrobial properties of chitosan-based-nanocomposite with potential applications for food packaging, J. Polym. Environ. 28 (4) (2020) 1216–1236.
[49] S. Bashiri, B. Ghanbarzadeh, A. Ayaseh, J. Dehghannya, A. Ehsani, Preparation and characterization of chitosan-coated nanostructured lipid carriers (CH-NLC) containing cinnamon essential oil for enriching milk and anti-oxidant activity, LWT Food Sci. Technol. 119 (2020) 108836.
[50] A. Pavinatto, A.V. de Almeida Mattos, A.C.G. Malpass, M.H. Okura, D.T. Balogh, R.C. Sanfelice, Coating with chitosan-based edible films for mechanical/biological protection of strawberries, Int. J. Biol. Macromol. 151 (2020) 1004–1011.
[51] J. Liu, S. Tian, X. Meng, Y. Xu, Effects of chitosan on control of postharvest diseases and physiological responses of tomato fruit, Postharvest Biol. Technol. 44 (3) (2007) 300–306.
[52] V. Saharan, A. Mehrotra, R. Khatik, P. Rawal, S.S. Sharma, A. Pal, Synthesis of chitosan-based nanoparticles and their *in vitro* evaluation against phytopathogenic fungi, Int. J. Biol. Macromol. 62 (2013) 677–683.
[53] E.L. de Souza, et al., Efficacy of a coating composed of chitosan from Mucor circinelloides and carvacrol to control *Aspergillus flavus* and the quality of cherry tomato fruits, Front. Microbiol. 6 (JUL) (2015) 1–9.
[54] F.I. Abo El-Ela, W.H. Hassan, A.M. Amer, S.I. El-Dek, Antifungal activity of chitosan polymeric nanoparticles and correlation with their pH against *Mucor circinelloides* causing mucormycosis, along with *Penicillium notatum* and *Aspergillus* species, Curr. Microbiol. 81 (1) (2024) 1–15.
[55] A.G. Luque-Alcaraz, et al., Enhanced antifungal effect of chitosan/pepper tree (*Schinus molle*) essential oil bionanocomposites on the viability of *Aspergillus parasiticus* spores, J. Nanomater. 2016 (2016).
[56] D. Chouhan, A. Dutta, A. Kumar, P. Mandal, C. Choudhuri, Application of nickel chitosan nanoconjugate as an antifungal agent for combating Fusarium rot of wheat, Sci. Rep. 12 (14518) (2022) 1–21.
[57] E. Ghasemian, A. Naghoni, B. Tabaraie, T. Tabaraie, *In vitro* susceptibility of filamentous fungi to copper nanoparticles assessed by rapid XTT colorimetry and agar dilution method, J. Mycol. Med. 22 (4) (2012) 322–328.
[58] E. Martínez-Batista, C.A. González-Arias, R.M. Velázquez-Estrada, J.A. Herrera-González, P. Gutiérrez-Martínez, *In vitro* and *in vivo* antifungal activity of chitosan and identification of potentially toxigenic fungi in stored maize of Nayarit, Mexico, Rev. Mex. Ing. Química 23 (2) (2024) 1–12.
[59] H.N. Cuong, N.C. Minh, N. Van Hoa, D.H. Giang, N. Van Hieu, P.V. Nam, Antifungal activity of squid pen chitosan nanoparticles against three fungal pathogens in various citrus fruits *in vitro* and *in vivo*, Coatings 12 (2) (2022).
[60] C. Rueda, M. Cuenca-Estrella, O. Zaragoza, Paradoxical growth of *Candida albicans* in the presence of caspofungin is associated with multiple cell wall rearrangements and decreased virulence, Antimicrob. Agents Chemother. 58 (2) (2014) 1071–1083.
[61] V. Loiko, J. Wagener, The paradoxical effect of echinocandins in *Aspergillus fumigatus* relies on recovery of the β-1,3-glucan synthase Fks1, Antimicrob. Agents Chemother. 61 (2) (2017) 1–11.
[62] I.F. Olawuyi, J.J. Park, J.J. Lee, W.Y. Lee, Combined effect of chitosan coating and modified atmosphere packaging on fresh-cut cucumber, Food Sci. Nutr. 7 (3) (2019) 1043–1052.
[63] D. Meng, et al., Antifungal activity of chitosan against *Aspergillus ochraceus* and its possible mechanisms of action, Int. J. Biol. Macromol. 158 (2020) 1063–1070.
[64] R. Li, et al., High molecular weight chitosan oligosaccharide exhibited antifungal activity by misleading cell wall organization via targeting PHR transglucosidases, Carbohydr. Polym. 285 (2022) 119253.
[65] A. Kapoor, D.N.M.B. Narasimhan, Antibacterial and antifungal evaluation of synthesized 9,12-octadecadienoic acid derivatives, Der Pharm. Lett. 6 (5) (2014) 246–251.
[66] S.A. Bukhari, M. Salman, M. Numan, M.R. Javed, M. Zubair, G. Mustafa, Characterization of antifungal metabolites produced by *Lactobacillus plantarum* and *Lactobacillus coryniformis* isolated from rice rinsed water, Mol. Biol. Rep. 47 (3) (2020) 1871–1881.
[67] F.D. Bello, C.I. Clarke, L.A.M. Ryan, H. Ulmer, T.J. Schober, K. Stro, Improvement of the Quality and Shelf Life of Wheat Bread by Fermentation with the Antifungal Strain *Lactobacillus Plantarum* FST 1 . 7, vol. 45, 2007, pp. 309–318.
[68] U. Schillinger, J.V. Villarreal, Inhibition of *Penicillium nordicum* in MRS medium by lactic acid bacteria isolated from foods, Food Control 21 (2) (2010) 107–111.
[69] J. Zhao, F. Wei, W. Xu, X. Han, Enhanced antibacterial performance of gelatin/chitosan film containing capsaicin loaded MOFs for food packaging, Appl. Surf. Sci. 510 (2020) 145418.
[70] E. Azadbakht, Y. Maghsoudlou, M. Khomiri, M. Kashiri, Development and structural characterization of chitosan films containing *Eucalyptus globulus* essential oil: potential as an antimicrobial carrier for packaging of sliced sausage, Food Packag. Shelf Life 17 (2018) 65–72.
[71] W. Zhang, W. Jiang, Antioxidant and antibacterial chitosan film with tea polyphenols-mediated green synthesis silver nanoparticle via a novel one-pot method, Int. J. Biol. Macromol. 155 (2020) 1252–1261.
[72] P. Zimet, et al., Physico-chemical and antilisterial properties of nisin-incorporated chitosan/carboxymethyl chitosan films, Carbohydr. Polym. 219 (2019) 334–343.